www.sciencemag.org/cgi/content/full/333/6038/62/DC1

Supporting Online Material for

Reconfigurable Knots and Links in Chiral Nematic Colloids

Uroš Tkalec,* Miha Ravnik, Simon Čopar, Slobodan Žumer, Igor Muševič*

*To whom correspondence should be addressed. E-mail: uros.tkalec@ijs.si (U.T.); igor.musevic@ijs.si (I.M.)

Published 1 July 2011, *Science* **333**, 62 (2010)
DOI: 10.1126/science.1205705

This PDF file includes:

Other Supporting Online Material for this manuscript includes the following:
(available at www.sciencemag.org/cgi/content/full/[vol]/[issue]/[page]/DC1)

Movies S1 to S3

Supporting Online Material

Reconfigurable Knots and Links in Chiral Nematic Colloids

Uroš Tkalec*, Miha Ravnik, Simon Čopar, Slobodan Žumer, Igor Muševič*

*To whom correspondence should be addressed. E-mail: uros.tkalec@ijs.si (U.T.);

igor.musevic@ijs.si (I.M.)

This PDF file includes:

Materials and Methods

Figures S1 to S2

Table S1

References 34 to 43

Captions for Movies S1 to S3

Other Supporting Online Material for this manuscript includes the following:

Movies S1 to S3

Materials and Methods

1. Preparation of colloidal dispersions and liquid crystal cells

Silica microspheres (Bangs Laboratories) were used in all experiments. The mean diameter of the particles is $d = (4.72 \pm 0.02)\mu m$ and it was determined by imaging a large number of colloidal particles under an optical microscope, followed by the particle size analysis. The surface of the particles was coated with a monolayer of N,N-dimethyl-N-octadecyl-3-aminopropyltrimethoxy-silyl chloride (DMOAP). This renders the silica surface hydrophobic (low energy) and is known to induce very strong perpendicular alignment of 4-cyano-4'-pentyl-1,1'-biphenyl (5CB) liquid crystal at the interface (*34*). The colloidal particles were first put into 1 wt% water solution of DMOAP. After several minutes they were separated from solution, rinsed with distilled water several times and dried at 110 °C for 30 min to remove the residual solvent. Finally, DMOAP-coated particles were suspended in the nematic phase of 5CB liquid crystal (Merck) at a typical concentration of 1 wt%.

The surface of the indium tin oxide (ITO) covered glass substrates was cleaned in an ultrasonic bath and thoroughly rinsed with deionized water and *iso*-propanol. After drying in an oven at 80 °C for 20 min, the substrates were spin-coated with a polyamic acid solution of PI-2555 (Nissan Chemicals) to produce a 100 nm thick layer. The coated substrates were soft-baked at 80 °C for 45 min to evaporate the solvent and subsequently hard-baked at 250 °C for 90 min to finalize the imidization reaction. At last, the polyimide coating was unidirectionally rubbed several times with a velvet cloth to obtain a homogeneous planar alignment for 5CB molecules.

The sample cell was prepared by sandwiching a droplet of colloidal dispersion between two perpendicularly oriented polyimide-covered ITO glass substrates to ensure 90° helical winding of the 5CB director throughout the sample, thus providing a weakly chiral nematic environment. The cell thickness was set to 6 μm using the mylar spacers. The local thickness of the cell was measured with a spectrophotometer USB2000+ (Ocean Optics) using a standard interference technique before the colloidal dispersion was filled in by the capillary flow. The handedness of the twisted nematic profile was determined by using a combination of polarizing optical microscopy and optical compensator (*35*) with a 530 nm phase shift.

2. *Laser tweezers manipulation*

Laser tweezers are widely used to manipulate colloidal particles in isotropic fluids (*36*) and topological defects in anisotropic fluids (*37-39*). We have utilized laser tweezers setup (LTM-N2000-A, Aresis), built around inverted optical microscope (Nikon Eclipse TE2000-U), equipped with a motorized stage (Prior OptiScan II), high numerical aperture water immersion objective (Nikon NIR Apo 60x/1.0w), halogen lamp and Ar+ ion laser source (Coherent, Innova 90C-4, λ = 514.5 nm, P_{max} = 1.7 W). The laser beam was spatially controlled with a pair of acousto-optic deflectors (AA Optoelectronic DTSXY-400-532), driven by a beam steering controller (BSC-01, Aresis), which enables creation of multiple optical traps and their precise positioning. A custom software (*40*) (Tweez v2.1, Aresis), running on a personal computer, connected with the beam steering controller and fast CMOS camera (PixeLINK PL-A741), was used to manipulate optical traps and to record experimental videos. The maximum power of a diffraction limited Gaussian laser beam in the sample plane was varied between 20 and 60 mW. Color images were acquired by digital camera (Nikon Coolpix E5400).

We have assembled two-dimensionally entangled colloidal structures by controlled fusion of separated defect loops using laser tweezers. Examples of creation and manipulation of small entangled colloidal clusters are shown in Fig. S1. We applied a low-power optical trap of 30 mW to manipulate the particles inside the liquid-crystalline matrix and a short high-power 60 mW laser pulse to perform a rapid temperature rise to locally melt a small nematic volume. Heat conduction following the pulse yields a temperature quench in the nematic phase. Since the entanglement of disclination lines using the temperature quench is a stochastic process, we have repeated the quenching several times to obtain the desired configuration. Initially, the optical trap was used as an optical scissors, which cut defect strands by heating the surrounding nematic fluid and then the same trap operated as an optical solder that reconnects the cut off strands during the slow cooling of the heated nematic region.

3. *Numerical modeling of nematic colloids*

To model nematic colloids, we employ a continuum, single elastic constant Landau-de Gennes approach, based upon the tensor order parameter, Q_{ij}. This approach naturally accounts for

effective elasticity of the liquid crystal, variations in the magnitude of the order, and possible biaxiality. The free energy is taken to be

$$F = + \int_{LC} \left\{ \frac{A}{2} Q_{ij} Q_{ij} + \frac{B}{3} Q_{ij} Q_{jk} Q_{ki} + \frac{C}{4} \left(Q_{ij} Q_{ij} \right)^2 \right\} dV + \frac{L}{2} \int_{LC} \frac{\partial Q_{ij}}{\partial x_k} \frac{\partial Q_{ij}}{\partial x_k} dV + \frac{W}{2} \int_{CS} \left(Q_{ij} - Q_{ij}^0 \right)^2 dS,$$

where LC denotes an integral over the volume occupied only by the liquid crystal and CS denotes an integral over the surface of the colloidal particles. The first term is the bulk free energy dependent on the order parameter that describes a first order transition between an isotropic and a nematic phase, with $A = a(T - T_{NI}^*)$, where a, B, and C are material constants, T is a temperature, and T_{NI}^* is the nematic-isotropic super-cooling temperature. The second term describes the energy cost of distortions in the liquid crystalline order; L is a corresponding elastic constant. The final term describes the interaction of the liquid crystal with the surfaces of the colloidal particles where W represents the strength of the surface anchoring and Q_{ij}^0 is the order parameter preferred by the surface, which we take to be homeotropic. At the top and bottom surfaces we assume strong homogeneous planar anchoring in two mutually perpendicular directions, which impose 90° twisted profile of the director. On side surfaces of the simulation box, we take fixed twisted profile of the nematic as obtained from separate calculations of an empty 90° twisted nematic cell without particles. Note that weak chiral nematic ordering field is not intrinsic (there is no chiral term in free energy), but it is solely induced by the confining surfaces.

We obtained minimum energy configurations by solving a system of coupled partial differential equations with appropriate boundary conditions using an explicit Euler finite difference relaxation algorithm on a cubic mesh (*41*). In order to produce the desired entangled defect patterns, initial conditions were chosen for the tensor Q_{ij} corresponding to the locally isotropic phase (random director spins) within the localized regions surrounding the particles. Separately, also analytical Ansætze for initial conditions of Q_{ij} were constructed to span disclination lines along the desired directions. The surface of each particle was defined by the set of mesh points contained within a spherical shell with thickness equal to the mesh resolution. Mesh points outside the surface were updated according to the bulk Ginzburg-Landau equations, appropriate

boundary conditions were imposed on the surface points and no computations were performed for the interior points. For computational efficiency, the effects of fluid flow were neglected in the relaxation dynamics as these are not expected to effect the equilibrium configurations.

Material parameters were chosen to match a typical nematic liquid crystal and were taken to be: $L = 4 \times 10^{-11}\mathrm{N}$, $A = -0.172 \times 10^{6}\mathrm{J/m^3}$, $B = -2.12 \times 10^{6}\mathrm{J/m^3}$, $C = 1.73 \times 10^{6}\mathrm{J/m^3}$, particle diameter d = 1 μm, cell thickness h = 2 μm, homeotropic anchoring strength $W = 1 \times 10^{-2}\mathrm{J/m^2}$, and mesh resolution $\Delta x = 10$ nm (cubic mesh).

4. Topological analysis of nematic braids and knot classification

The ability to discern and classify different kind of knots and links is an essential requirement for understanding entangled networks of disclination loops. The mathematical field of knot theory offers powerful tools for detecting and classifying different knots (*24*), typically by transforming a knot projection into a special polynomial formula, which depends on the knot type but not on any particular projection. Comparing this polynomial with those enumerated in *Table of knot invariants* (*29*) enables the indentification of the knot type from a given projection. One of the most applicable families of polynomials are Jones polynomials (*2*, *24*) that constitute strong topological invariants and represent invaluable tool for analyzing the vast majority of simpler knots.

A major effort of our topological analysis was to classify the observed nematic braids on $p \times q$ particle arrays by using the concept of Jones polynomials. Such rectangular lattices comprehend a collection of unit tangles that are located in a grid layout with $(p-1) \times (q-1)$ dimension. This enables a relatively simple view over the phase space of possible nematic braids. Thus, we enumerated all $3^{(p-1)\times(q-1)}$ braids with a computer algorithm and subsequently calculated their self-linking numbers (*42*).

To determine the knot type of a certain configuration, we implemented computer algorithm for finding a knot's Jones polynomial based on the skein theory approach, as introduced by L. Kauffman (*43*). Remarkably, the unit tangles, recognized in the plane of a twisted nematic cell, exactly correspond to the basic units of knot diagrams that are used in the calculation procedure

of the Kauffman bracket polynomial $\langle K \rangle$ (*24*). This method involves recursive generation of all possible zero-crossing knot states S_i, where all the crossing sites in a knot diagram K are eliminated. Each crossing may be replaced by one of the two possible states: $A \equiv \asymp$ or $A^{-1} \equiv)($, resulting in $|S_i|$ disconnected loops. This information is sufficient to calculate the Kauffman polynomial $X(K)$ in the variable A by using a computer program (*24*):

$$X(K) = (-A)^{-3w(K)}\langle |K| \rangle = (-A)^{-3w(K)} \sum_i \langle S_i|K\rangle (-A^2 - A^{-2})^{|S_i|-1}.$$

Here, the sum covers all possible states of S_i, $\langle S_i|K\rangle$ denotes the product of all A and A^{-1} at the crossing sites, and $w(K)$ corresponds to the integer writhe of the initial knot diagram. An example of Kauffman states generation and Kauffman polynomial calculation is schematically illustrated in Fig. S2. The Jones polynomial is finally obtained by the substitution $A \rightarrow t^{-1/4}$ and compared with polynomials in the enumerated *Table of knot invariants* (*29*).

Jones polynomials are unique for prime knots and links with up to 9 crossings (*24*), which is the regime of knots and links that we worked with. At higher number of crossings, the Jones polynomials can fail to distinguished different knots and links but nevertheless still substantially narrow down the number of candidates for a given topological configuration. We have analyzed $p \times q$ particle arrays with p, $q \in [2, 3, 4]$ and found more than 70 different topological types. Since the configurations on smaller arrays always reappear on a larger array, we present the collection of topologically different configurations on a 4×4 particle array in Table S1. Remarkably, the great majority of identified configurations belongs to relatively small fraction of knots and links with 7 or less crossings. More than 29% of them are equivalent to unknot, 18.2% are unlinks, 12.4% represent prime knots, and 22.8% of phase space is occupied by prime links. The remaining portion of 17.5% is covered by more complex composite knots and links. In sum, the majority of prime knots and links with minimal crossing numbers up to 7 have already been observed on a 4×4 particle array.

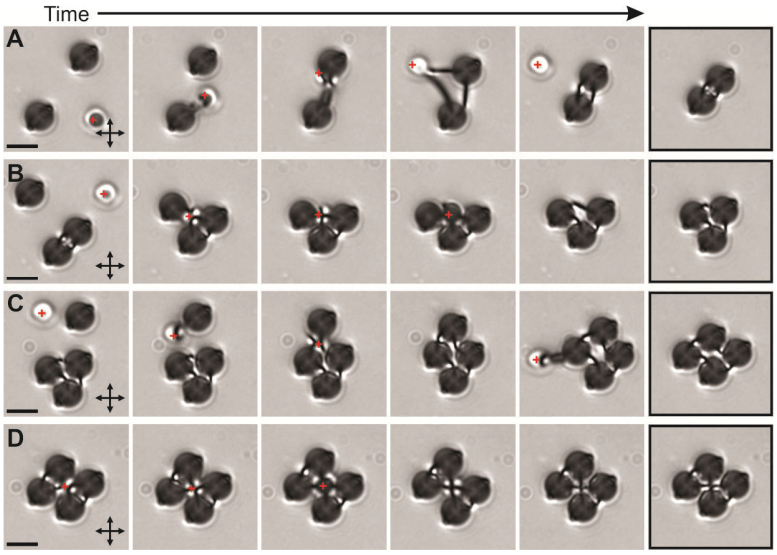

Figure S1. Creation and manipulation of small entangled colloidal clusters using laser tweezers. (**A**) Two separated microspheres with encircled disclination rings were positioned close to each other and entangled by a single defect loop. The defect rings were cut by the laser beam and rejoined into dimer configuration. (**B**) The third particle was attached from the side, forming a tight elastic bond among the three colloidal particles. (**C**) When the fourth particle with its ring was attached to the entangled trimer, several tetramer configurations were possible. In the first example, the defect lines merged four colloidal particles into encircled cluster. (**D**) The encircled tetramer was further transformed into the crossed tetramer by creating an inter-particle crossing of defect strands. Scale bars correspond to 5 μm, a red cross shows the position of the optical trap and the crossed double arrows show the orientation of the polarizers.

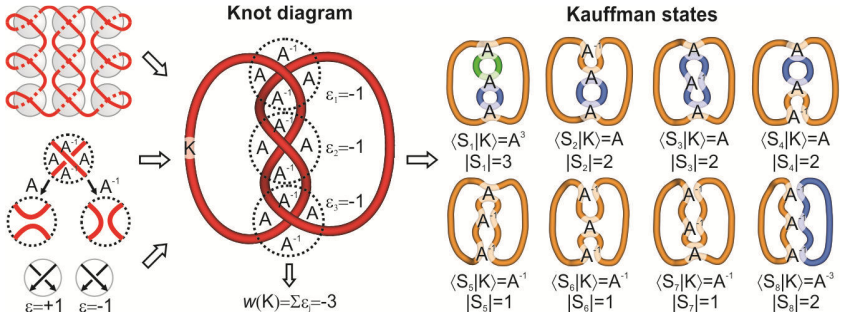

Figure S2. Construction of Kauffman states for left-handed trefoil knot on a 3 × 3 particle array. Firstly, the physical conformation is transformed into a knot diagram K, where all the crossings are identified and an integer writhe $w(K)$ is calculated. Then, all possible zero-crossing states are produced, which determine a state of the knot as a whole. Here, $\langle S_i|K\rangle$ denotes the product of all A and A^{-1} at the crossing sites and $|S_i|$ corresponds to the number of loops in the resulting link diagram. Finally, the Kauffman polynomial of a given knot is $X(K) = -A^{16} + A^{12} + A^4$.

Knots		**2-component links**		**3-component links**		**4-component links**	
Type	Counts	Type	Counts	Type	Counts	Type	Counts
0_1	5756	0^2_1	3032	0^3_1	519	0^4_1	30
3_1	1698	2^2_1	3516	6^3_1	28	8^4_1	2
4_1	454	4^2_1	534	6^3_2	3	8^4_2	2
5_1	62	5^2_1	196	6^3_3	30	8^4_3	1
5_2	164	6^2_1	28	7^3_1	8	$L_{10}n_{104}$	1
6_2	16	6^2_3	60	8^3_4	3	$0_1+6^3_1$	2
6_3	12	7^2_5	12	8^3_7	6	$0_1+2^2_1\#2^2_1$	146
7_1	8	7^2_7	26	8^3_9	6	$3_1+2^2_1\#2^2_1$	4
7_4	4	7^2_8	12	8^3_{10}	3	$0^2_1+2^2_1$	102
7_5	12	8^2_1	2	$L_{10}n_{93}$	1	$0^2_1+4^2_1$	9
8_{19}	12	8^2_4	4	$0_1+2^2_1$	1158	$2^2_1+4^2_1$	10
$3_1\#3_1$	42	9^2_{53}	2	$0_1+4^2_1$	105	$4^2_1+4^2_1$	1
		0_1+3_1	400	$0_1+5^2_1$	21	$2^2_1\#6^3_3$	2
		0_1+4_1	60	$0_1+6^2_3$	4	$2^2_1\#2^2_1\#2^2_1$	67
		0_1+5_2	12	$0_1+3_1\#2^2_1$	12	$2^2_1\#2^2_1\#4^2_1$	16
		$0_1+3_1\#3_1$	2	$3_1+0^2_1$	26	**5-component links**	
		3_1+3_1	4	$3_1+2^2_1$	20	Type	Counts
		$3_1\#2^2_1$	282	$3_1+4^2_1$	4	$0^2_1+2^2_1\#2^2_1$	9
		$3_1\#4^2_1$	28	$2^2_1\#2^2_1$	652	$2^2_1+2^2_1\#2^2_1$	10
		$4_1\#2^2_1$	24	$2^2_1\#4^2_1$	104	$4^2_1+2^2_1\#2^2_1$	2
		$5_1\#2^2_1$	12	$2^2_1\#6^2_1$	4	$2^2_1\#2^2_1\#2^2_1\#2^2_1$	6
		$5_2\#2^2_1$	12	$2^2_1\#6^2_2$	4	**6-component links**	
				$4^2_1\#4^2_1$	7	Type	Counts
				$3_1\#2^2_1\#2^2_1$	32	$2^2_1\#2^2_1+2^2_1\#2^2_1$	1

Table S1. Distribution of knots and links on a 4×4 particle array. The designations of knots follow the standard notation C_i^N, where C indicates the minimal number of crossings, i distinguishes between different knot types and N represents the number of loops in multi-component links. Prime knots and links are designated by a single mark, whereas composite knots and links combine either a direct sum of two prime knots or links, denoted by »+«, or their connected sum, denoted by »#«. The counts represent the actual number of distinguished topological objects in a given particle array. All tabulated configurations were identified by numerical Jones polynomial calculation and direct comparison with polynomials in the enumerated *Table of Knot Invariants* (*29*).

References and Notes

1. C. C. Adams, *The Knot Book* (American Mathematical Society, Providence, 2004).

2. L. H. Kauffman, *Knots and Physics* (World Scientific Publishing, Singapore, ed. 3, 2000).

3. J. P. Sauvage, C. Dietrich-Buchecker, Eds., *Molecular Catenane, Rotaxanes and Knots: A Journey through the World of Molecular Topology* (Wiley, Weinheim, 1999).

4. K. S. Chichak *et al*., Molecular borromean rings. *Science* **304**, 1308 (2004). doi:10.1126/science.1096914 Medline

5. D. Han, S. Pal, Y. Liu, H. Yan, Folding and cutting DNA into reconfigurable topological nanostructures. *Nat. Nanotechnol.* **5**, 712 (2010). doi:10.1038/nnano.2010.193 Medline

6. P. G. de Gennes, *Scaling Concepts in Polymer Physics* (Cornell Univ. Press, New York, 1979).

7. L. Faddeev, A. J. Niemi, Stable knot-like structures in classical field theory. *Nature* **387**, 58 (1997). doi:10.1038/387058a0

8. W. T. M. Irwine, D. Bouwmeester, *Nat. Phys.* **4**, 716 (2008). doi:10.1038/nphys1056

9. M. R. Dennis, R. P. King, B. Jack, K. O'Holleran, M. J. Padgett, Isolated optical vortex knots. *Nat. Phys.* **6**, 118 (2010). doi:10.1038/nphys1504

10. A. D. Bates, A. Maxwell, *DNA Topology* (Oxford Univ. Press, Oxford, ed. 2, 2005).

11. D. Meluzzi, D. E. Smith, G. Arya, Biophysics of knotting. *Annu. Rev. Biophys.* **39**, 349 (2010). doi:10.1146/annurev.biophys.093008.131412 Medline

12. Y. Bouligand, Recherches sur les textures des états mésomorphes. 5. noyaux, fils et rubans de mœbius dans les nématiques et les cholestériques peu torsadés. *J. Phys. (Paris)* **35**, 215 (1974). doi:10.1051/jphys:01974003503021500

13. P. G. de Gennes, J. Prost, *The Physics of Liquid Crystals* (Oxford Science Publications, Oxford, 1993).

14. N. D. Mermin, The topological theory of defects in ordered media. *Rev. Mod. Phys.* **51**, 591 (1979). doi:10.1103/RevModPhys.51.591

15. P. Poulin, H. Stark, T. C. Lubensky, D. A. Weitz, Novel Colloidal Interactions in Anisotropic Fluids. *Science* **275**, 1770 (1997). doi:10.1126/science.275.5307.1770 Medline

16. H. Stark, Physics of colloidal dispersions in nematic liquid crystals. *Phys. Rep.* **351**, 387 (2001). doi:10.1016/S0370-1573(00)00144-7

17. D. G. Grier, A revolution in optical manipulation. *Nature* **424**, 810 (2003). doi:10.1038/nature01935 Medline

18. M. Yada, J. Yamamoto, H. Yokoyama, Direct observation of anisotropic interparticle forces in nematic colloids with optical tweezers. *Phys. Rev. Lett.* **92**, 185501 (2004). doi:10.1103/PhysRevLett.92.185501 Medline

19. I. Muševič *et al*., Laser trapping of small colloidal particles in a nematic liquid crystal: clouds and ghosts. *Phys. Rev. Lett.* **93**, 187801 (2004). doi:10.1103/PhysRevLett.93.187801 Medline

20. I. Muševič, M. Škarabot, U. Tkalec, M. Ravnik, S. Žumer, Two-dimensional nematic colloidal crystals self-assembled by topological defects. *Science* **313**, 954 (2006). doi:10.1126/science.1129660 Medline

21. T. Araki, H. Tanaka, Colloidal aggregation in a nematic liquid crystal: Topological arrest of particles by a single-stroke disclination line. *Phys. Rev. Lett.* **97**, 127801 (2006). doi:10.1103/PhysRevLett.97.127801 Medline

22. M. Ravnik *et al*., Entangled nematic colloidal dimers and wires. *Phys. Rev. Lett.* **99**, 247801 (2007). doi:10.1103/PhysRevLett.99.247801 Medline

23. Materials and methods are available as supporting material on *Science* Online.

24. V. V. Prasolov, A. B. Sossinsky, *Knots, Links, Braids and 3-Manifolds* (American Mathematical Society, Providence, 1997).

25. S. Čopar, S. Žumer, Nematic braids: Topological invariants and rewiring of disclinations. *Phys. Rev. Lett.* **106**, 177801 (2011). doi:10.1103/PhysRevLett.106.177801 Medline

26. J. H. White, Self-linking and the gauss integral in higher dimensions. *Am. J. Math.* **91**, 693 (1969). doi:10.2307/2373348

27. F. Wilczek, A. Shapere, Eds., *Geometric phases in physics* (World Scientific Publishing, Singapore, 1988).

28. D. M. Raymer, D. E. Smith, Spontaneous knotting of an agitated string. *Proc. Natl. Acad. Sci. U.S.A.* **104**, 16432 (2007). doi:10.1073/pnas.0611320104 Medline

29. J. C. Cha, C. Livingston, *KnotInfo: Table of Knot Invariants*, http://www.indiana.edu/~knotinfo (2011).

30. S. Mühlbauer *et al*., Skyrmion lattice in a chiral magnet. *Science* **323**, 915 (2009). doi:10.1126/science.1166767 Medline

31. J. Fukuda, S. Žumer, Quasi-two-dimensional Skyrmion lattices in a chiral nematic liquid crystal. *Nat. Commun.* **2**, 246 (2011). doi:10.1038/ncomms1250 Medline

32. D. R. Nelson, Condensed-matter physics: Vortices weave a tangled web. *Nature* **430**, 839 (2004). doi:10.1038/430839a Medline

33. R. G. Sharein, thesis, University of British Columbia (1998).

34. F. J. Kahn, G. N. Taylor, H. Schonhorn, Surface-produced alignment of liquid crystals. *Proc. IEEE* **61**, 823 (1973). doi:10.1109/PROC.1973.9171

35. M. Kleman, O. D. Lavrentovich, *Soft Matter Physics* (Springer, New York, 2003).

36. A. Ashkin, Optical trapping and manipulation of neutral particles using lasers. *Proc. Natl. Acad. Sci. U.S.A.* **94**, 4853 (1997). doi:10.1073/pnas.94.10.4853 Medline

37. I. I. Smalyukh, A. N. Kuzmin, A. V. Kachynski, P. N. Prasad, O. D. Lavrentovich, Optical trapping of colloidal particles and measurement of the defect line tension and colloidal forces in a thermotropic nematic liquid crystal. *Appl. Phys. Lett.* **86**, 021913 (2005). doi:10.1063/1.1849839

38. M. Škarabot *et al*., Laser trapping of low refractive index colloids in a nematic liquid crystal. *Phys. Rev. E Stat. Nonlin. Soft Matter Phys.* **73**, 021705 (2006). doi:10.1103/PhysRevE.73.021705 Medline

39. I. I. Smalyukh, A. V. Kachynski, A. N. Kuzmin, P. N. Prasad, Laser trapping in anisotropic fluids and polarization-controlled particle dynamics. *Proc. Natl. Acad. Sci. U.S.A.* **103**, 18048 (2006). doi:10.1073/pnas.0608698103 Medline

40. N. Osterman, TweezPal—Optical tweezers analysis and calibration software. *Comput. Phys. Commun.* **181**, 1911 (2010). doi:10.1016/j.cpc.2010.07.024

41. M. Ravnik, S. Žumer, Landau-de Gennes modelling of nematic liquid crystal colloids. *Liq. Cryst.* **36**, 1201 (2009). doi:10.1080/02678290903056095

42. R. D. Kamien, The geometry of soft materials: A primer. *Rev. Mod. Phys.* **74**, 953 (2002). doi:10.1103/RevModPhys.74.953

43. L. H. Kauffman, *Topology* **26**, 395 (1987). doi:10.1016/0040-9383(87)90009-7

Acknowledgments: U.T. thanks S. Herminghaus, S. Kralj, and S. Vrtnik for discussions. M.R. acknowledges support of the European Commission (EC) under the Marie Curie Program Active Liquid Crystal Colloids (ACTOIDS); content reflects only the authors views and not the views of the EC. The research was funded by Slovenian Research Agency under the contracts P1-0099, PR-00182, and J1-9728, and in part by the NAMASTE Center of Excellence.

Movie S1

This movie shows the assembly of two-dimensionally entangled colloidal cluster in a left-twisted nematic profile using laser tweezers. Two pairs of silica spheres (4.72 μm diameter), coated with DMOAP, are initially entangled by two separated disclination loops having a form of the double figure of eight. Using high-power optical trap the local temperature quench of the nematic fluid is performed in the vicinity of the particles, during which the two disclination loops join into a single ring. This structure can be further transformed into a tetramer with the crossed profile of the defect loops in the centre of the tetramer. Topologically, both configurations are equivalent to unknot. The isotropic phase appears black between crossed polarizers. The movable cross shows the position of an optical trap. (QuickTime: 173 kB).

Movie S2

This movie shows the creation of the Hopf link, the simplest nontrivial topological configuration that is made of two interlinked defect loops. The assembly process starts with two twisted disclinations loops, each having three crossings of the same type and being spanned over three neighboring colloidal particles. Using an optical trap one can simultaneously cut and rejoin the defect strands of both disclination loops at two rewiring sites and knit the Hopf link. (QuickTime: 226 kB).

Movie S3

This movie shows the assembly of the trefoil knot that can be entangled around seven colloidal particles. The separated defect rings gradually join into a single disclination loop using optical trap manipulation. The final configuration can be recognized as the trefoil knot with three nontrivial crossings in the middle particle row. (QuickTime: 361 kB).